

07,01

## Influence of combined treatment of the surface layer on the impact resistance of steel

© S.A. Atroshenko<sup>1,2</sup>, D.A. Gerashchenkov<sup>3</sup>, A.V. Kuznetsov<sup>4</sup>, G.G. Savenkov<sup>4,5</sup> M.S. Smakovakiy<sup>4</sup>

<sup>1</sup> Institute of Problems of Mechanical Engineering, Russian Academy of Sciences, St. Petersburg, Russia

<sup>2</sup> St. Petersburg State University, St. Petersburg, Russia

<sup>3</sup> Central Scientific Research Institute Of Structural Materials „Prometey“, St. Petersburg, Russia

<sup>4</sup> Armalit Machine-Building Plant, St. Petersburg, Russia

<sup>5</sup> St. Petersburg State Technological Institute (Technical University), St. Petersburg, Russia

E-mail: satroshe@mail.ru

Received December 7, 2023

Revised December 7, 2023

Accepted December 25, 2023

The results of a study of the influence of cold gas-dynamic spraying followed by laser processing of samples made of carbon steel 20 and stainless steel 08X18H10T on their dynamic (spall) strength under impact loading conditions at a strain rate of  $10^5 \cdot \text{s}^{-1}$  are presented. The influence of impact speed on the microstructure of samples and their spall strength was studied. It was shown that the dynamic (spall) strength of laser-treated samples after their gas-dynamic spraying changed little in relation to samples without treatment. The microstructure of the tested samples was studied. It has been established that a large amount of martensite is formed inside the ferritic grains of carbon steel during impact loading, and intense mechanical twinning develops in the austenitic grains of austenitic steel upon impact, with the largest number of twins observed in samples without laser treatment. In the spall crack zone of the treated stainless steel samples, areas of amorphization and melting were found.

**Keywords:** gas dynamic spraying, laser processing, steel, dynamic strength, microstructure, martensite, twins.

DOI: 10.61011/PSS.2024.02.57920.269

### 1. Introduction

Currently, in order to achieve high results in creating materials for products operating in extreme conditions, a discipline that provides functional surface properties is being actively developed: the so-called 2D materials. One of the methods that makes it possible to obtain this kind of material is the method of cold gas-dynamic spraying (CGDS) [1,2]. Cold spraying technology is based on the effect of the formation of a durable metal layer when a two-phase supersonic flow approaches a normally located surface [3], at a particle temperature significantly lower than their melting point. The CGDS method is of exceptional interest due to the low processing temperature, which excludes the presence of processes associated with changes in the chemical or phase composition. This makes it possible to obtain coatings that are completely consistent with the original powders. Such coatings have sufficient thickness, adhesive strength and a given stoichiometric composition for subsequent heat treatment. The relatively low temperature of the transfer process prevents degradation of the composition or structure of the original powder components, as well as of the metal substrate material.

Subsequent processing of the sprayed layer using a laser beam is a kind of laser doping of the surface layer of the source material, which leads to the targeted formation of structure [4].

In general, the combined two-stage technology ensures the creation of intermetallic composite coatings and bulk additive materials with controlled composition and structure using cold gas-dynamic spraying of a precursor coating and subsequent heat and laser treatment.

Laser doping, along with other high-energy methods (for example, electron beam), is used as a surface treatment of metals and alloys that are poorly strengthened by traditional chemical-thermal methods [5].

During laser doping the increase in microhardness and other operational characteristics of the surface layer of the material is achieved not only due to structural (as at laser hardening) and phase transformations in the laser effected zone, but also due to the creation of a new alloy that differs from the matrix material in chemical composition [6].

The use of laser processing of a pre-applied precursor layer makes it possible to obtain modified layer with the controlled chemical composition on the surface of the substrate. In turn, the chemical composition regulation is carried out by changing the thickness of the precursor coa-

ting and varying the laser processing modes. Measurement of the temperature of aluminum-based powder particles during cold gas-dynamic spraying of coatings showed that the temperature of particles in the gas flow at the stagnation temperature 500–600°C for aluminum powder does not exceed 40°C. The layer is formed in two stages: at the first stage, a precursor coating is applied using the cold gas-dynamic spraying method, at the second stage, a doped layer is formed under the influence of laser. The authors [7–10] studied the composition and properties of a nickel-alloyed layer on the surface of low-carbon steel. The results of X-ray diffraction analysis indicate the formation of a solid solution and an intermetallic compound in the formed layer of the FCC lattice.

There is a large range of metal materials used for the manufacture of machine parts that experience extreme (dynamic, temperature, etc.) external influences, which requires their resistance to such, in particular, shock loads.

At the same time, it is known that any modification of the surface of metals and alloys by various high-energy methods leads (for example, under conditions of plane-wave impact loading) to change in their dynamic characteristics [11–13] and impact resistance [14]. This is due to the presence of weak region of the modified material, namely the boundary of the strengthened layer (or coating) — substrate. However, it is unclear how the reinforced layer will behave under high-intensity impact loads, even if it is located on the back side of the impact accepted surface.

There is also no information about how the strengthened layer located on the free surface affects the spallation strength of the material as a whole. There is no doubt that the influence of the strengthened layer on the properties of the material shall be felt. It was noted in [15] that the behavior of materials with sprayed surface layer turned out to be more complex than expected. According to the authors opinion, this is a consequence of the difference in the properties of the main coating material and its near-surface layer, since it is known that diffusion processes change the chemical composition of the near-surface layer. The fact is that a sample with a surface-hardened layer can be considered as a kind of composite with a sandwich structure: a thin strengthened layer — ultra-thin interface — a thick viscous substrate. The mechanical properties of the material on both sides of the interface differ significantly; modulus of elasticity may also vary, although only slightly. Therefore, some local contact stresses can be created at the interface, which can change the entire course of the loading process development. Besides, at the interface, temperature or load changes can lead to the formation of micro-/macrocracks and delaminations. In principle, this can lead to both a change in the dynamic characteristics, including the spallation strength of the material, and to change in the mechanisms of deformation and fracture. To measure the tensile strength of interfaces between coatings (hardened layers) of micron thickness and substrates, in recent years the method of spallation induced by a high-speed impact or laser pulse was used [16–19].

The purpose of this paper was to evaluate changes in the dynamic (spallation) strength and structure of the material in disk-shaped samples made of carbon steel 20 and stainless steel 08Cr18N10T. One side of the disk was processed by a combined method (cold gas-dynamic spraying and subsequent laser processing), after which the samples were exposed to a flat impactor at a speed  $V = 220–350$  m/s.

## 2. Materials and research methods

The materials studied were carbon steel 20 and austenitic stainless steel 18Cr10NiTi. Powder A10-01 ( $Al + Al_2O_3$ ) was applied to one side of each disk with a diameter of 92 mm and thickness of 10 mm using the cold gas-dynamic spraying method by Dimet-403 unit (manufactured by „OTsPN“ LLC, Obninsk). Aluminum oxide in this case stabilized the deposition process. The sprayed layer was 60–80  $\mu\text{m}$  thick. After application, the sprayed surface was processed in laser complex „Fabrika“ (Russia) (Figure 1, *a*). Laser power during processing is 200 W, scanning speed is 100 mm/s, scanning step is 75  $\mu\text{m}$ , spot diameter is about 100  $\mu\text{m}$  with insignificant defocusing. The processing algorithm has a staggered nature (for a more uniform distribution of heating) (Figure 1, *b*).

After laser processing the corundum melted and went to the surface; thus, there was no corundum in the intermetallic layer; the thickness of the intermetallic layer was 80–100  $\mu\text{m}$ . The indicated temperature and speed parameters of the technological process were determined in paper [15].

Plane-wave impact loading of processed and unprocessed disks was carried out on experimental pneumatic gun of 57 mm caliber with a double-diaphragm shutter. The gun operates with compressed air and can create pressure up to 15 MPa. A complete description of the experimental setup is given in [20]. The use of gas gun makes it possible to obtain stable and easily monitored impact speeds  $V_0$  in the range of 50 to 500 m/s. Maximum tensile stresses (spallation strength) were determined only on samples unprocessed with laser or on processed samples with minimally ground layer (so that the signal could be

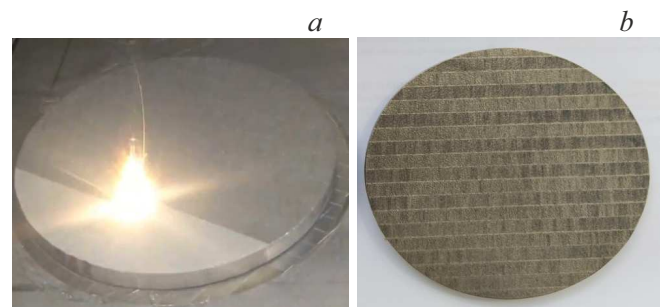


**Figure 1.** *a*) Laser processing of the sprayed surface and *b*) type of processed surface.

taken from this surface). The interferometer VISAR was used to record the free surface velocity. A single-mode and single-frequency neodymium laser Verdi-2 with built-in frequency doubler was used as a radiation source in the interferometer. The radiation wavelength was  $0.53 \mu\text{m}$ .

Interference patterns were processed only before the beginning of the spallation pulse [20–22]. From the obtained dependences of the free surface speed, the maximum free surface speed  $V_1$ , the minimum free surface speed  $V_2$  before the beginning of the spallation pulse and the time of decay of the free surface speed from  $V_1$  to  $V_2$  were determined. During testing some samples experienced separation of the spallation plate. Maximum tensile stresses and deformation rates were determined using the formulas

$$\sigma_p = 0.5\rho_0 c_0 (V_1 - V_2), \quad \dot{\varepsilon} = \frac{1}{2c_0} \cdot \frac{\partial V_1}{\partial t},$$

where  $\sigma_p$  — maximum tensile stress,  $\rho_0$  — density,  $c_0$  — volumetric speed of sound,  $V_1$  — maximum free surface speed,  $V_2$  — minimum free surface speed before the spallation pulse,  $\dot{\varepsilon}$  — deformation rate. In the case where spallation occurs,  $\sigma_p$  corresponds to the spallation strength.

Studies of the structure in the optical microscope Axio-Observer Z1 M were carried out in bright field and in contrast C-DIC (differential-interference contrast with circular polarization). Since the measurement of phase areas on a microsection in accordance with the Cavalieri principle [23] can be replaced by the measurement of segments per each phase, the specific phase interface was determined using linear analysis:  $S_{AB} = 2Z^{AB}/L$ , where  $L$  — total length of the measuring line;  $Z^{AB}$  — the number of points of the measuring line intersection with phase interfaces A and B. The microhardness of steel was determined using Shimadzu series HMV-G microhardness tester (using the Vickers method) at a load of 100 g.

### 3. Experimental results and discussion

#### 3.1. Impact experiments

##### 3.1.1. Steel 20

As a result of impact experiments, the maximum tensile stresses for steel 20 samples processed by laser were determined. The range of their changes was within  $\sigma_p = 1.1–1.5 \text{ GPa}$  at deformation rates  $\dot{\varepsilon} = 1.05 \cdot 10^4–1 \cdot 10^5 \text{ s}^{-1}$ . Examples of loading diagrams for samples with unprocessed surface (impact speed  $V = 222$  and  $355 \text{ m/s}$ ) are shown in Figure 2 (curves 1 and 3, respectively).

The maximum tensile stresses on the processed samples with ground surface were in the range  $\sigma_p = 1.32–1.62 \text{ GPa}$  at deformation rates  $\dot{\varepsilon} = 7.2 \cdot 10^4–1.1 \cdot 10^5 \text{ s}^{-1}$ . The example of loading diagram for sample with processed surface (impact speed  $V = 306 \text{ m/s}$ ) is shown in the Figure (curve 2). Thus, the maximum tensile stresses (spallation strength) increased by 4–20%.

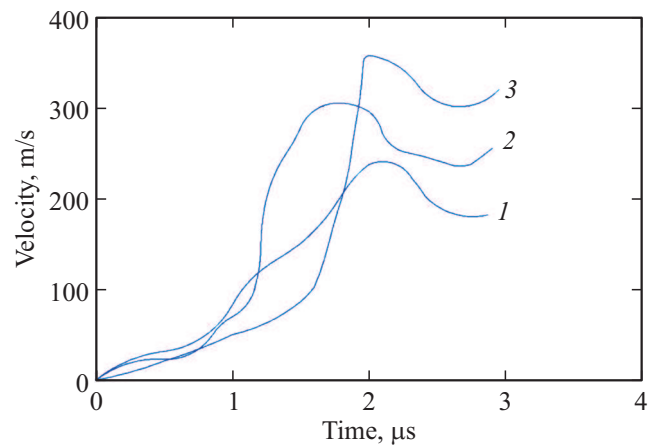


**Figure 2.** Time profiles of free surface speed of steel 20: curve 1 —  $V = 222 \text{ m/s}$  and 3 —  $V = 355 \text{ m/s}$  without surface laser processing; 2 —  $V = 306 \text{ m/s}$  with laser processing and ground surface.

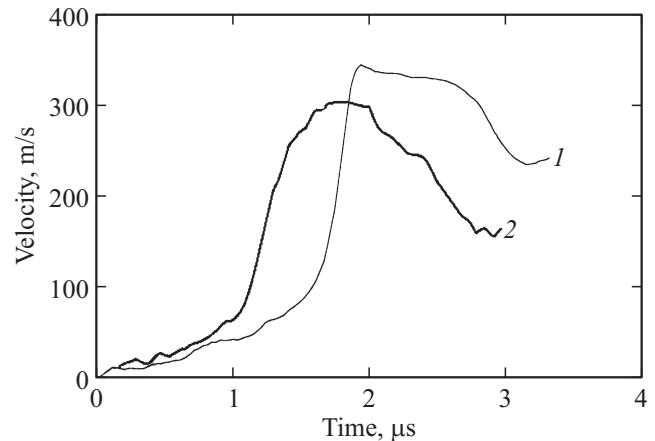


**Figure 3.** Loading diagrams for samples of stainless steel 18Cr10NiTi: curve 1 — with surface without laser processing,  $V = 343 \text{ m/s}$ ; 2 — laser processed surface, ground layer,  $V = 304 \text{ m/s}$ .

##### 3.1.2. Stainless steel 18Cr10NiTi

As a result of impact experiments the maximum tensile stresses for unprocessed samples were determined. The interval of their changes lay in the region  $\sigma_p = 1.8–2.2 \text{ GPa}$  at deformation rates  $\dot{\varepsilon} = (1.8–2.1) \cdot 10^5 \text{ s}^{-1}$ . An example of loading diagram for sample with unprocessed surface (impact speed  $V = 343 \text{ m/s}$ ) is shown in Figure 3 (curve 1).

The maximum tensile stresses on the processed surface with ground layer were in the region  $\sigma_p = 1.95–2.46 \text{ GPa}$  at deformation rates  $\dot{\varepsilon} = (2.1–2.5) \cdot 10^5 \text{ s}^{-1}$ . The example of loading diagram for sample with ground surface (impact speed  $304 \text{ m/s}$ ) — in Figure 2 (curve 2).

Thus, the strength characteristics after coating and laser processing of this layer changed little (maximum tensile stresses (spallation strength) increased by 8–15%). I.e., cold gas-dynamic spraying followed by laser processing of

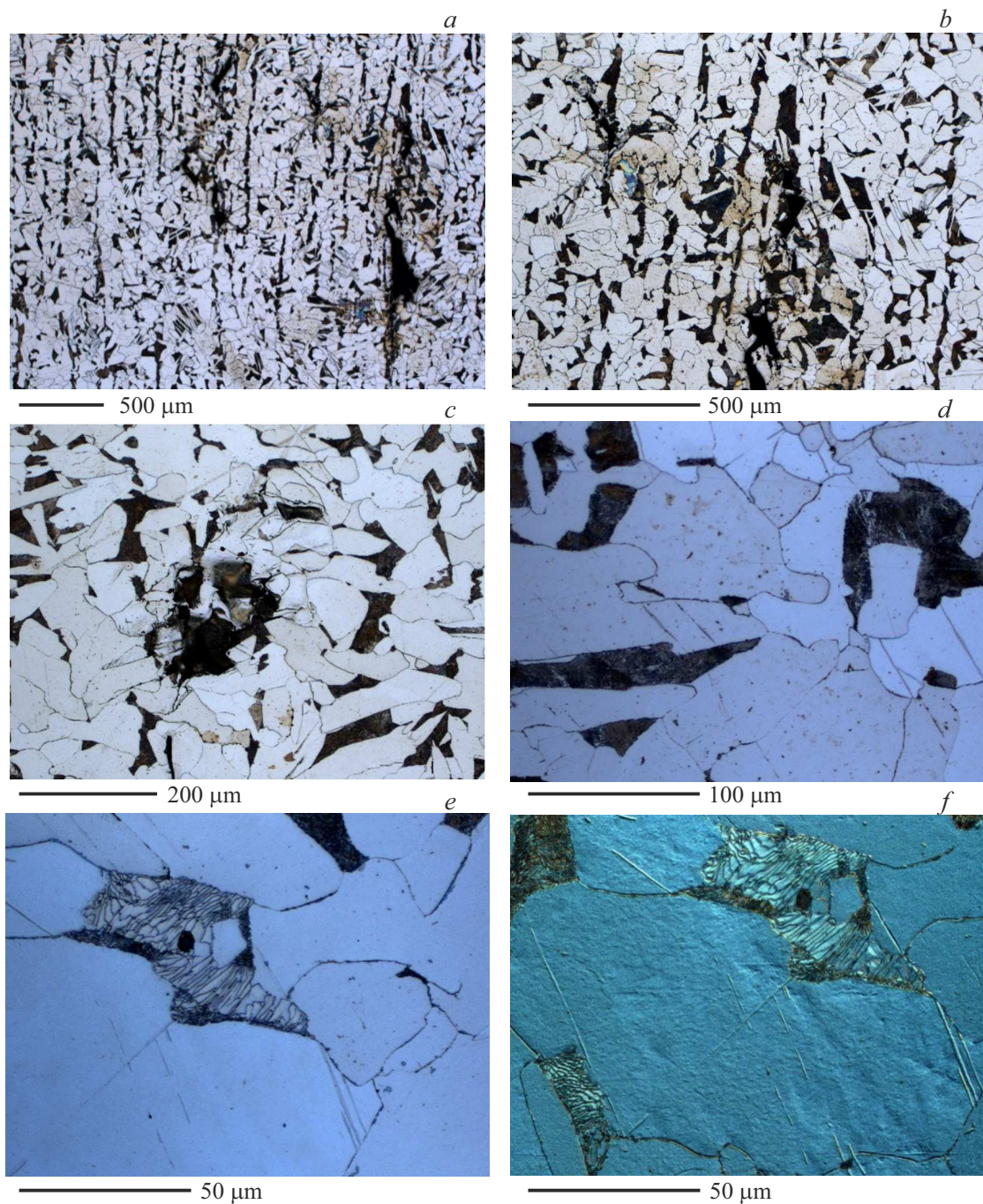


**Figure 4.** Structure of steel 20 coated without laser processing ( $V = 222$  m/s): *a*)  $\times 50$ , *b* and *c*)  $\times 200$ , *d*)  $\times 500$ , *e*)  $\times 1000$ , *f*)  $\times 1000$  C.DIC).

the back surface had virtually little effect on the spallation strength of both carbon and stainless steel.

### 3.2. Study of microstructure

#### 3.2.1. Steel 20

In the initial state (without laser processing), the structure of steel 20 after loading at speed  $V = 222$  m/s is grains of ferrite and lamellar pearlite (Figure 4).

It can be seen that the cracks run along the pearlite strips (Figure 4, *a* and *b*), located in the direction of preliminary mechanical processing (rolling or forging). The quantitative components of steel 20 after impact loading are presented in Table 1; the pearlite grain size is smaller than of the ferrite, and it is often located along the boundaries of the ferrite grain, along which cracks occur.

Pearlite and ferrite, as well as martensite and ferrite are taken as phases A and B [23].

**Table 1.** Quantitative characteristics of steel 20 structure after laser processing and impact loading

| Steel    | $V$ , m/s   | Layer, $\mu\text{m}$ | $D_{\text{pearlite}}$ , $\mu\text{m}$ | $d_{\text{ferrite}}$ , $\mu\text{m}$ | $h_{\text{pearlite}}$ , $\mu\text{m}$ | Slip | $S_{\text{PF}}$ , $\text{m}^{-1}$ | $S_{\text{MF}}$ , $\text{m}^{-1}$ |
|----------|-------------|----------------------|---------------------------------------|--------------------------------------|---------------------------------------|------|-----------------------------------|-----------------------------------|
| Steel 20 | 222 initial | 0                    | 52.9                                  | 81.5                                 | 1.02                                  | +    | $0.03 \cdot 10^6$                 | $0.04 \cdot 10^6$                 |
|          | 286 polish  | 0                    | 41.3                                  | 76.6                                 | 0.69                                  | +    | $0.06 \cdot 10^6$                 | $0.20 \cdot 10^6$                 |
|          | 303         | 51.3                 | 48.8                                  | 65.5                                 | 0.45                                  | +    | $0.04 \cdot 10^6$                 | $0.33 \cdot 10^6$                 |
|          | 351         | 94.1                 | 49.6                                  | 54.1                                 | 0.58                                  | +    | $0.06 \cdot 10^6$                 | $0.26 \cdot 10^6$                 |

Note. Layer — size of laser layer,  $V$  — loading rate,  $D_{\text{pearlite}}$  — pearlite grain size,  $d_{\text{ferrite}}$  — ferrite grain size,  $h_{\text{pearlite}}$  — interlamellar spacing in pearlite, Slip — slip strips,  $S_{\text{PF}}$  — specific surface of pearlite-ferrite interface,  $S_{\text{MF}}$  — specific surface of martensite-ferrite interface.

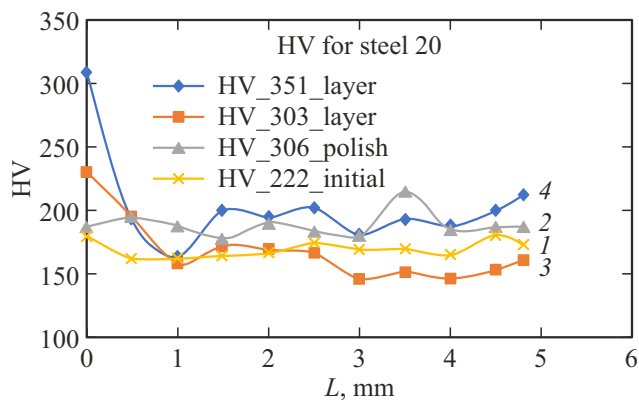


**Figure 5.** Panorama of changes in the hardness of steel 20 across the target from the free surface to the loaded one after impact with speeds: curve 1 —  $V = 222$  m/s in the initial state, without laser exposure; 2 —  $V = 306$  m/s after laser exposure and polishing of the laser layer; 3 —  $V = 303$  m/s after laser processing; 4 —  $V = 351$  m/s after laser exposure.

A panorama of the change in Vickers hardness across the target is shown in Figure 5. From the presented panorama it is clear that at speed  $V = 222$  m/s in the initial state — without laser exposure, the maximum hardness is observed at the edges of the sample, and in the middle of the sample the scatter is quite large: the decrease reaches 20 units, this is due to the heterogeneity of the structure — the presence of pearlite and ferrite of different hardness, as well as the presence of cracks.

The structure of steel 20 after laser processing of the coating and impact loading at speed of 286 m/s is shown in Figure 6. The entire laser layer was ground off on both sides, so it is absent.

After loading, the spallation plate was separated. Spallation cracks (Figure 6, *a*) run along the boundaries of ferrite grains and along pearlite plates (Figure 6, *c*). A large amount of martensite is present (Figure 6, *b* and *d*). With loading rate and laser exposure increasing, pearlite and ferrite grains were refined, and their scattering also decreased, i.e. they became more equiaxed, and the interlamellar spacing in pearlite also decreased, i.e. it became more dispersed. Analysis of steel samples for carbon revealed a layer depleted in carbon and a very thin layer enriched

in carbon inside the spallation zone, which indicates mass transfer of carbon from the adjacent zone to the fracture area [24–28]. The amount of pearlite increased, and the amount of martensite increased significantly. In the zone of interference of unloading waves, where negative pressure (tension) operates, the phase transformations are observed, which are the material reaction to short-term exposure to negative pressure [29–33].

The panorama of changes in the steel 20 hardness across the target after laser exposure and the laser layer polishing after loading at speed of 286 m/s (Figure 5) demonstrates a relatively uniform hardness distribution throughout the thickness of the sample and along the edges, only in the middle of the sample there is a spike in hardness by 30 units. The average hardness of this sample turned out to be higher than when loaded at speed of 222 m/s without laser exposure. This is due to laser processing, although the laser layer was ground off, as well as large amount of martensite formed (Table 1)

The structure of steel 20 after laser exposure on the coating and loading at speed of 303 m/s is shown in Figure 7.

After loading, the spallation plate was separated. The laser layer with an average thickness of  $50 \mu\text{m}$  is full with cracks along the loading direction (Figure 7, *a* and *d*). The inside the target run along the boundaries of ferrite grains and along pearlite grains (Figure 7, *b*). The spallation cracks are shown in Figure 7, *c*. With loading rate and laser exposure increasing, pearlite dissolved (crushing of its grains) (Figure 7, *e*) — the amount of pearlite decreased, but the amount of martensite increased (Figure 7, *f*) (Table 1). At loading rate of 303 m/s the size of the ferrite grain decreased with the same scattering as at lower speed, the size of the pearlite grain increased slightly with significant scattering, and the interlamellar spacing turned out to be the smallest among all tested samples, i.e. the most dispersed pearlite is observed at this speed and laser exposure.

The panorama of the steel 20 hardness change across the target (from the layer to the untreated surface) after laser exposure and after loading at speed of 303 m/s (Figure 5) shows the highest hardness in the laser processed layer; at the other end of the target (through thickness) the hardness is much lower — by 60 units. On average, at loading rate of 303 m/s, the hardness turned out to be at the level of the

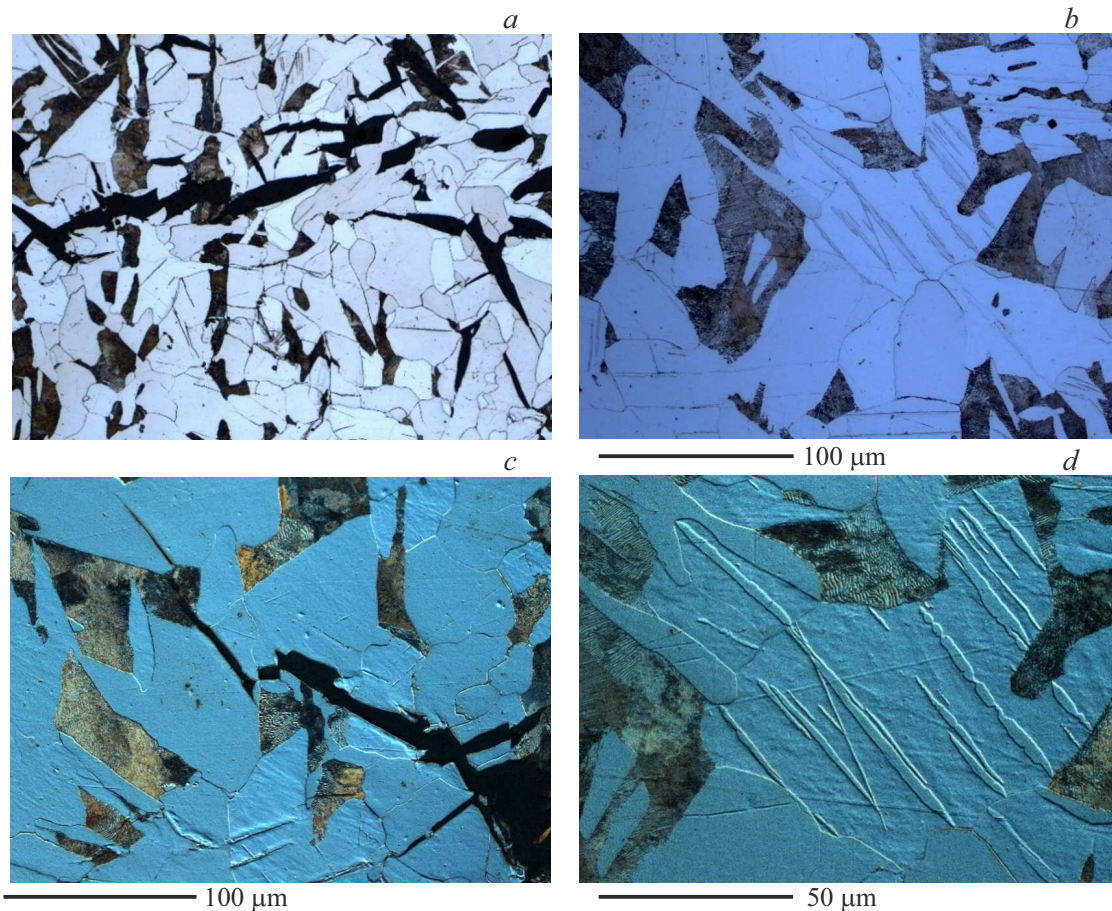


**Figure 6.** Structure of steel 20 after laser exposure and loading at speed of 286 m/s: *a*)  $\times 200$ , *b*)  $\times 500$ , *c*)  $\times 500$  C\_DIC, *d*)  $\times 1000$  C\_DIC).

sample loaded at speed of 222 m/s without laser loading, but without strong scattering in the thickness of the sample. The decrease in hardness compared to the sample loaded at speed of 286 m/s can be explained by the presence of cracks in the laser layer, despite the maximum amount of martensite in this sample.

The structure of steel 20 after laser exposure and loading at speed of 351 m/s is shown in Figure 8. The separation of the spallation plate is also observed. The laser layer (Figure 8, *a*) with average thickness of  $95\ \mu\text{m}$  looks like a combination of large molten and crystallized droplets, and unlike the previous case (Figure 7, *a*) it turned out to be without cracks. The spallation fracture is shown in Figure 8, *b*. The amount of pearlite increased and of the martensite decreased (Figure 8, *c* and *d*) compared to loading at lower speed (Table 1). The loading rate and laser exposure increasing led to the ferrite grain refinement and decrease in its scattering — the structure became more equiaxed, while the pearlite grain changed little, but the scattering also decreased. The interlamellar spacing increased slightly. At this deformation rate the vortex structures are observed near the laser layer (Figure 8, *e*). There are also dislocations slip lines (Figure 8, *f*).

Using the SIAMS structure analyzer, the martensite structure score was determined according to GOST 8233 — Structure score 10: macroacicular.

The panorama of changes in steel 20 hardness across the target (from the layer to the unprocessed surface) after laser exposure after loading at speed of 351 m/s demonstrates the maximum hardness in the laser layer; at a distance of 0.5 mm it decreases and changes little over the target thickness. On average, the hardness turned out to be maximum in this sample, both over thickness and in the layer, among all tested steel 20 samples. This is due to the fact that the laser layer has no cracks and is the largest in thickness, as well as with the maximum loading rate.

### 3.2.2. Steel 18Cr10NiTi

A large number of twins of different sizes and directions are observed in the structure of the sample. As it is known, the mechanism of plastic deformation in the form of twinning, the implementation of which requires the application of high shear stresses, is characteristic of FCC metals under explosive and impact loads [34–37].

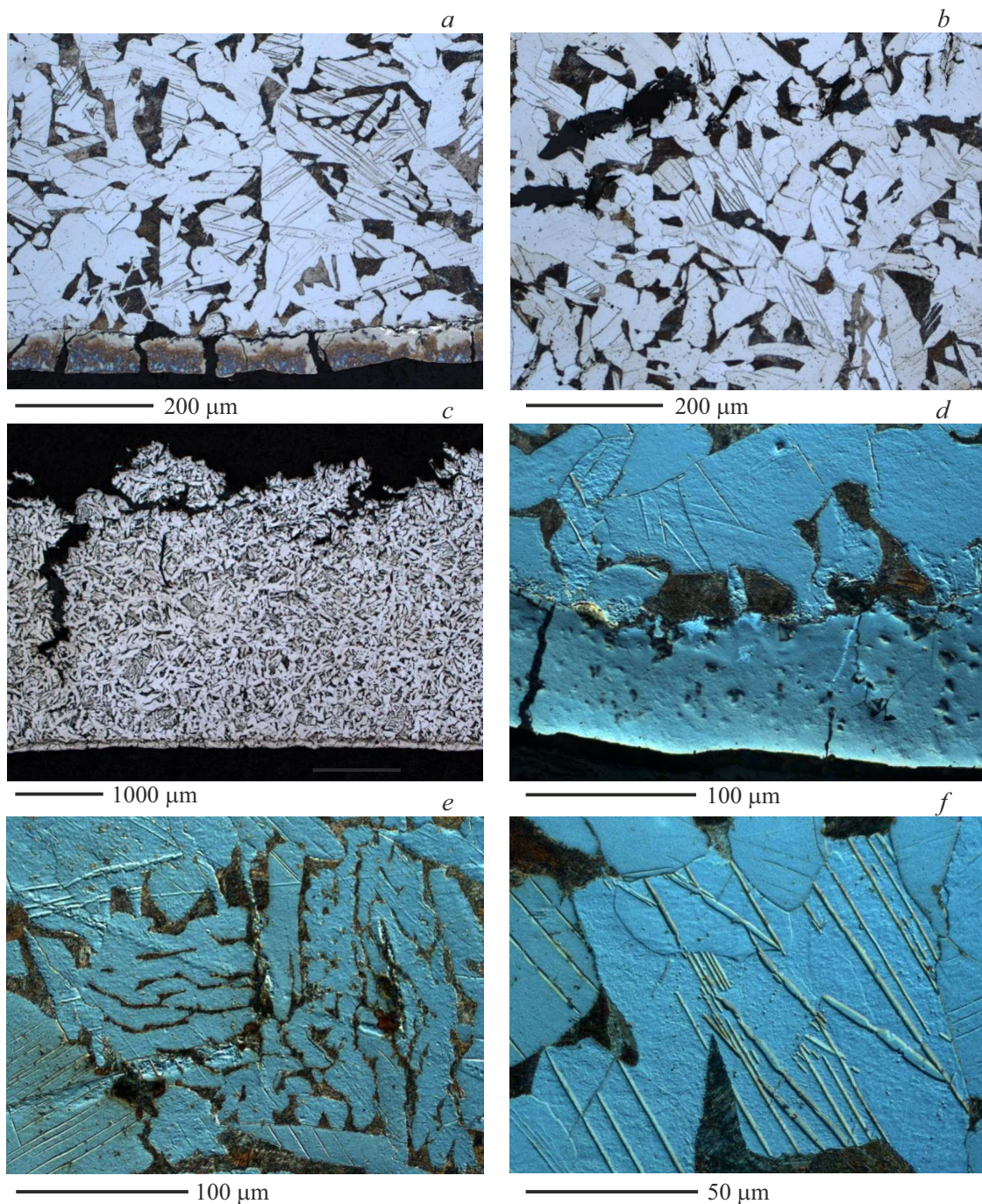


**Figure 7.** Structure of steel 20 after laser exposure and loading at speed of 303 m/s: *a* and *b*)  $\times 200$ , *c*)  $\times 25$ , *d* and *e*)  $\times 500$  C.DIC, *f*)  $\times 1000$  C.DIC).

Cracks are located in the direction of preliminary deformation and often occur on inclusions of intermetallic compounds. The cracks and pores have a round, elongated shape (Figure 9, *a*). They are located in the direction of shock wave propagation.

The panorama of hardness changes of all tested samples is presented in Figure 10. For the initial (without laser processing) sample loaded at speed of 343 m/s, the hardness shows a rather large scattering (20 units) over the thickness

of the target *L*, despite that the average hardness of this sample was the highest of all tested. This is probably due to the highest speed of impact on the target (343 m/s), although without laser processing. The scattering over the target thickness is associated with the presence of a large number of cracks and brittle phases.

The structure of steel 18Cr10NiTi after laser processing of the coating and impact loading at speed of 276 m/s is shown in Figure 11.

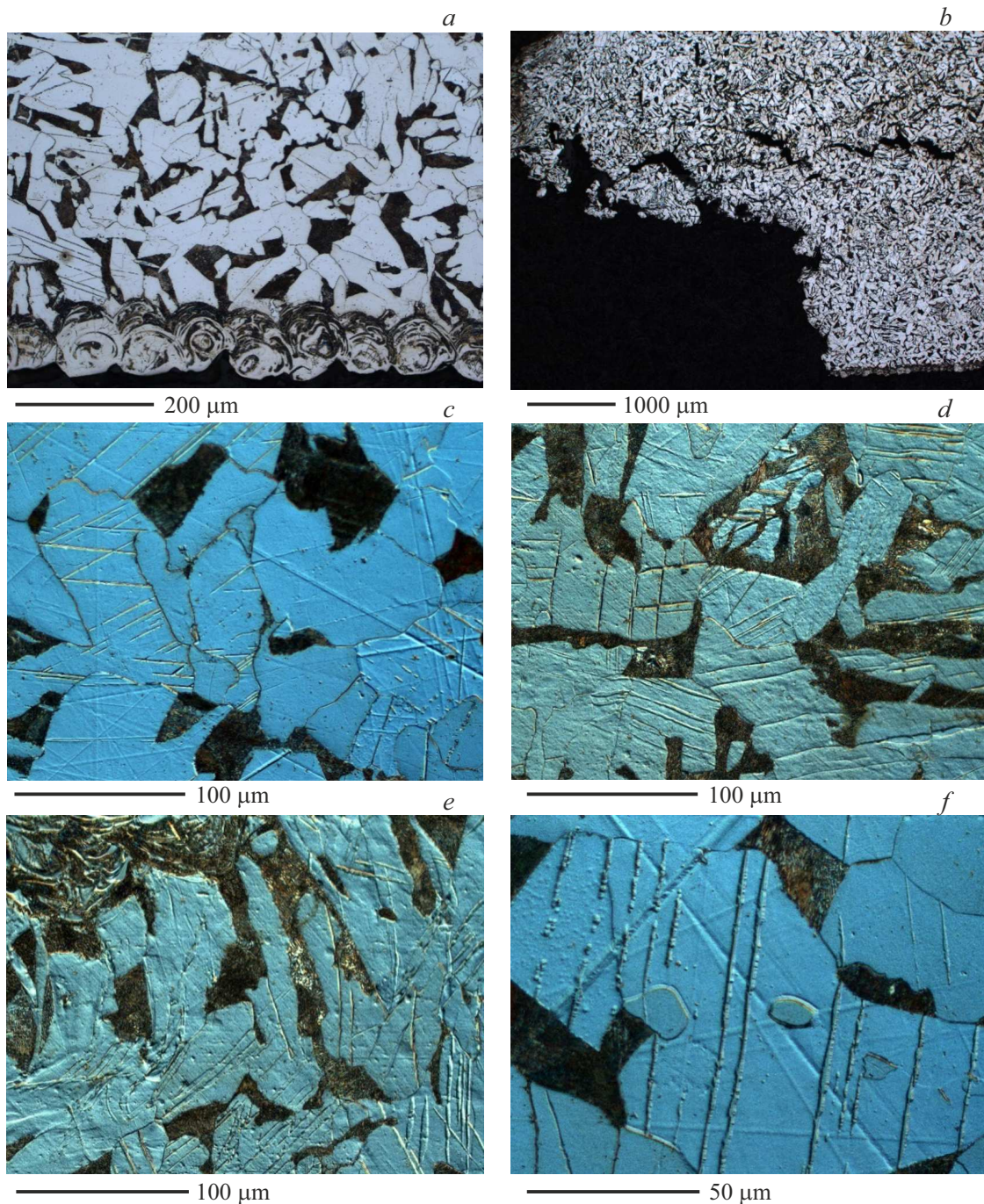


**Figure 8.** Structure of steel 20 after laser exposure and loading at speed of 351 m/s: *a*)  $\times 200$ , *b*)  $\times 25$ , *c*, *d* and *e*)  $\times 500$  C.DIC, *f*)  $\times 1000$  C.DIC).

The laser layer has an average thickness of  $80\mu\text{m}$  (Figure 11, *a* and *c*) in some places has individual cracks, sometimes at the interface with the base metal (Figure 11, *c*). Cracks caused by impact loading are located along (Figure 11, *b*) the direction of preliminary deformation and in the direction of the shock wave propagation. Chains of intermetallic phases along which cracks pass are visible (Figure 11, *a* and *c*). The cracks often have an oval shape (Figure 11, *d*), as in the initial state (without laser

processing), many twins are observed. But their number decreased, and the average size increased (Table 2) (which is associated with decrease in impact speed and, as a consequence, decrease in shear stresses). In some places near the crack a dendritic structure was discovered (Figure 11, *b*), which indicates local melting in this area. In the spallation zone, in the zone of interference of unloading waves, where negative pressure (tension) operates, phase transformations, amorphization, and recrystallization are observed, which

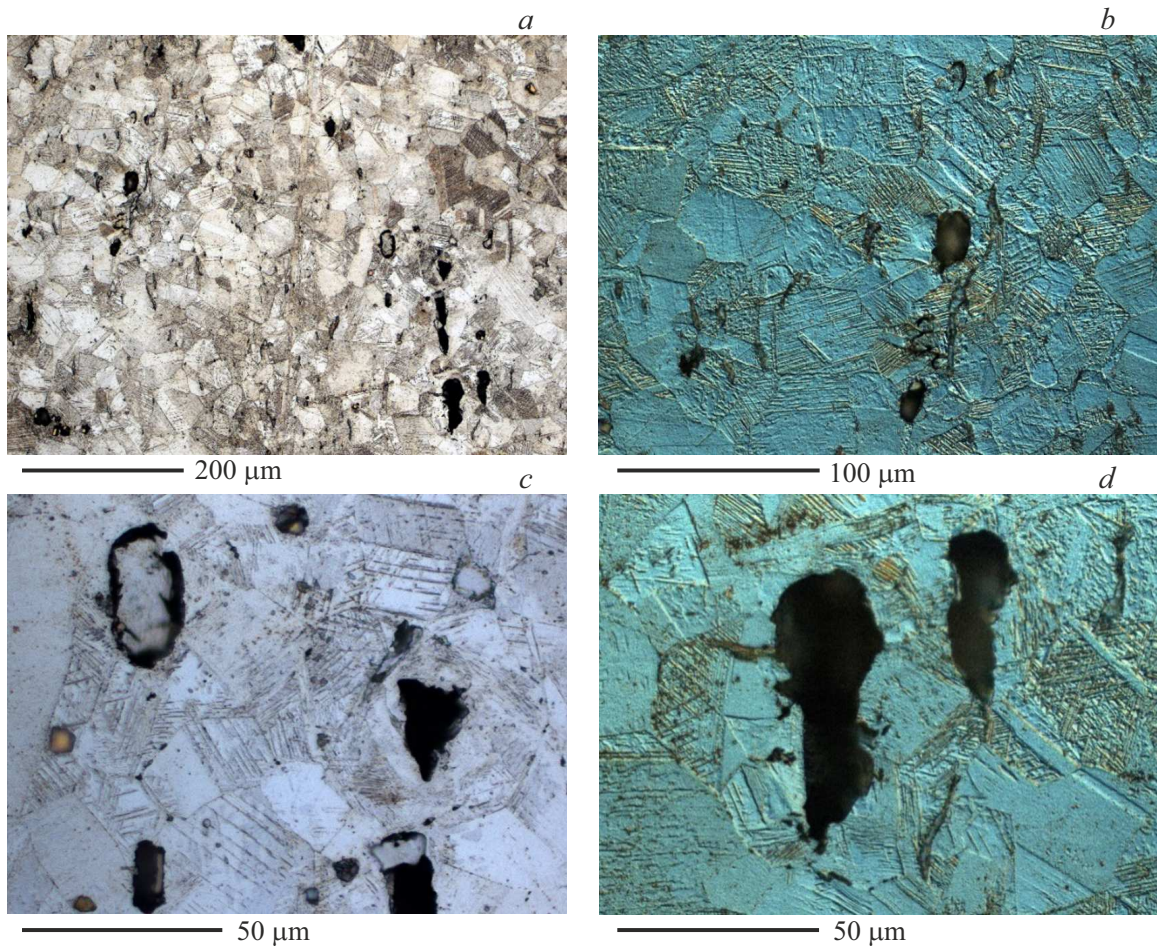


**Figure 9.** Structure of steel 18Cr10NiTi after impact loading at speed of 343 m/s in the initial state — without laser exposure: a)  $\times 200$ , b)  $\times 500$  C-DIC, c)  $\times 1000$ , d)  $\times 1000$  C-DIC).

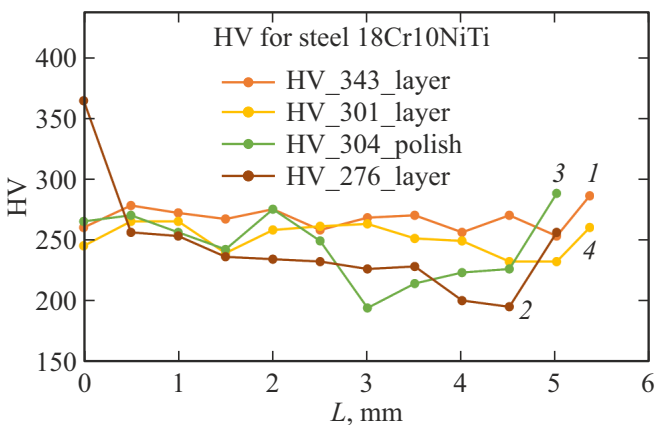


**Figure 10.** Panorama of the change in steel 18Cr10NiTi hardness across the target from the free surface to the loaded one: curve 1 — after impact with speed of 343 m/s in the initial state — without laser exposure; 2 — after laser processing and impact loading at speed of 276 m/s; 3 — after laser exposure, polishing of the laser layer and impact loading at speed of 304 m/s; 4 — after laser exposure and impact loading at speed of 301 m/s.

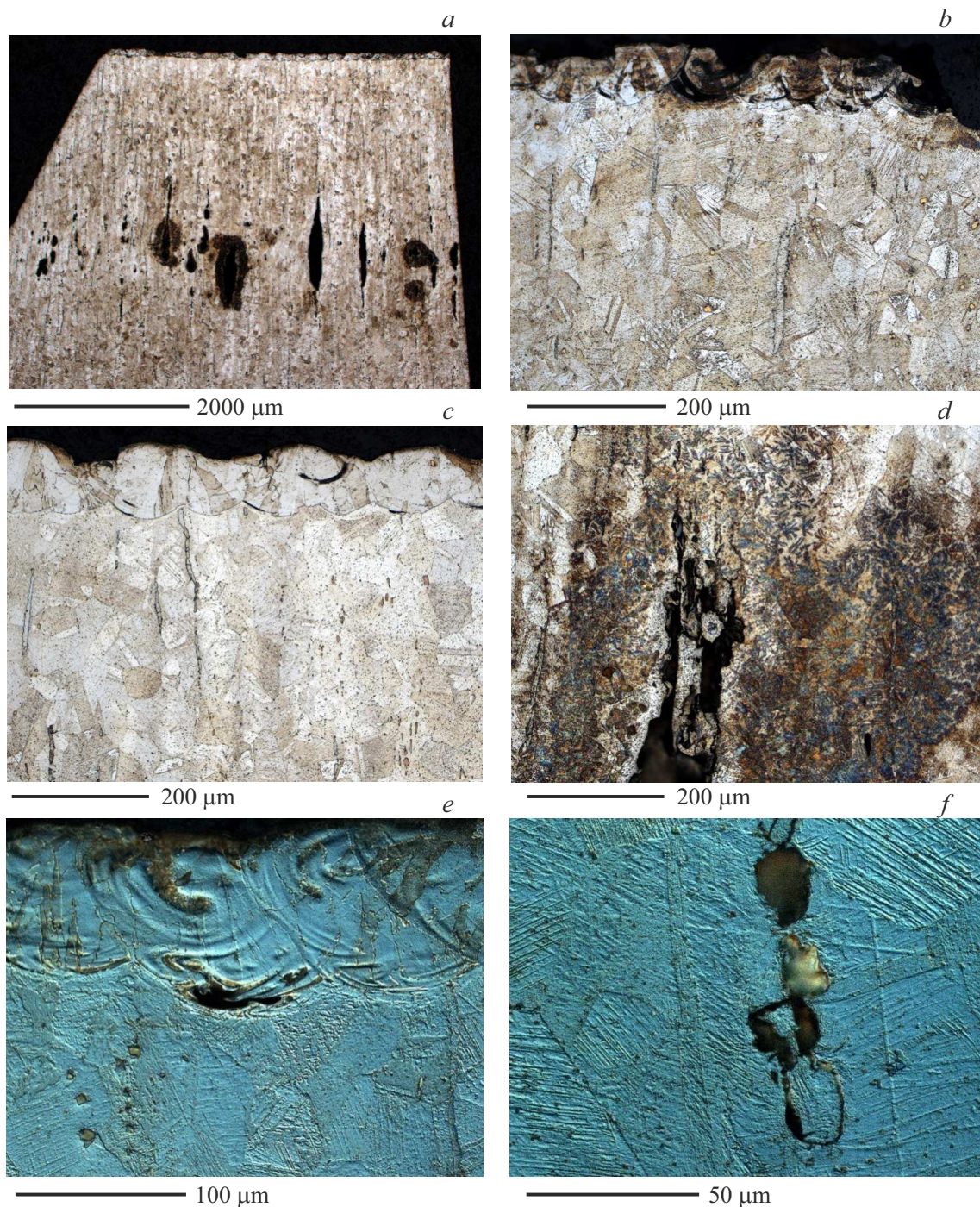
are the reaction of the material to short-term exposure to negative pressure[27–36].

Table 2 shows the quantitative characteristics of the microstructure of the under study measured using an Axio Vision analyzer [23].

Phases A and B are taken to be twin and austenite. As can be seen from the Table, the number of twins increases with loading rate increasing, which is confirmed by photographs of the microstructure (Figure 9, Figures 11–13), and the more twins are observed, the higher the strength of the material is [25–26], which is confirmed by microhardness data (Figure 10).

The panorama of hardness changes (Figure 10) for this sample (276 m/s) demonstrates the highest hardness in the laser coating layer; at distance of 0.5 mm from the layer, the hardness decreases significantly, and further over the thickness of the sample it changes little. This is probably due to laser exposure, which creates a layer in the form of crystallized droplets.

The structure of steel 18Cr10NiTi after laser exposure and impact loading (the laser layer is ground off, so it is absent) at speed of 304 m/s is shown in Figure 12. The



**Figure 11.** Structure of steel 18Cr10NiTi after laser exposure and impact loading at speed of 276 m/s: *a*)  $\times 25$ , *b*, *c* and *d*)  $\times 200$ , *e*)  $\times 500$  C.DIC, *f*)  $\times 1000$  C.DIC).

cracks run from the ground off layer (Figure 12, *b* and *c*). Individual spallation cracks are observed (Figure 12, *a* and *d*). An area of amorphization was discovered in the area of the spallation zone.

Around the cracks, areas of melting with dendritic structure are observed (Figure 12, *c*). Cracks appear along the boundaries of austenite grains near the laser processing surface (Figure 12, *e*), where the accumulation of

intermetallic compounds is observed. With increase in the loading rate, increase in the number of twins (Figure 12, *e* and *f*), and decrease in their sizes are observed, as well as decrease in the size of the austenite grain and its scattering.

From the panorama of changes in hardness (Figure 10) it is clear that the hardness of this sample, loaded at rate of 304 m/s with a laser-ground layer, changes slightly along the thickness of the sample.

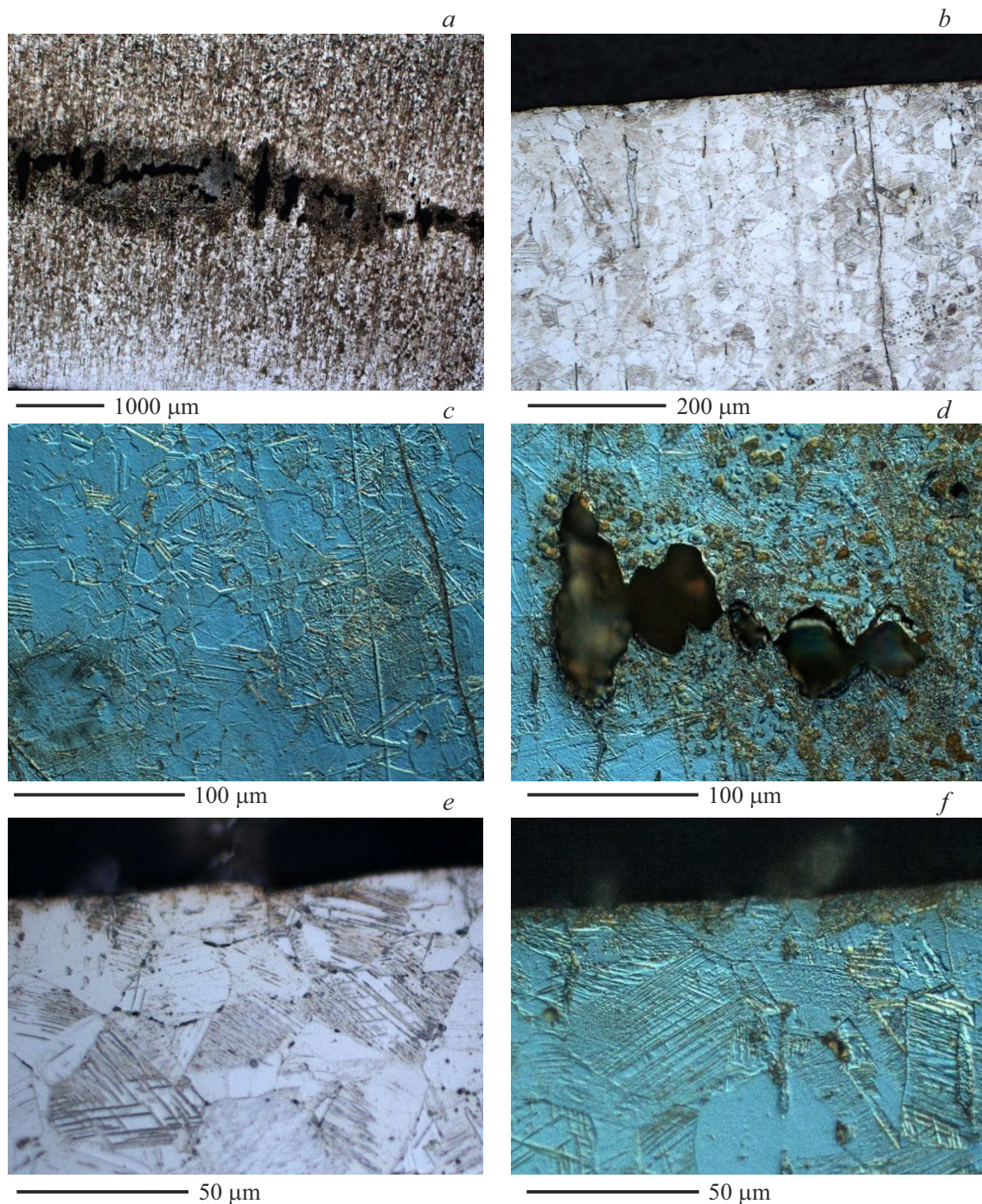


**Figure 12.** Structure of steel 18Cr10NiTi after laser exposure and impact loading at speed of 304 m/s: *a*)  $\times 25$ , *b*)  $\times 200$ , *c* and *d*)  $\times 500$  C.DIC, *e*)  $\times 1000$ , *f*)  $\times 1000$  C.DIC).

The structure of steel 18Cr10NiTi after laser exposure and impact loading at speed of 301 m/s is shown in Figure 13.

The laser layer with an average thickness of  $125\ \mu\text{m}$  is shown in Figure 13, *a* and *b*. The cracks are located in the direction of preliminary deformation (Figure 13, *a*), a dendritic structure is observed in the area of cracks (Figure 13, *c* and *d*), which indicates local melting; the size

of austenite grains also increased. Areas of amorphization were discovered (Figure 13, *e* and *f*). The number of twins decreased and their size increased, and the size of the austenite grain and its scattering increased.

The panorama of the change in hardness of this sample (Figure 10) at a loading rate of 301 m/s shows a very large scattering (almost 35 units) of hardness over the target thickness. This is due to the presence of large

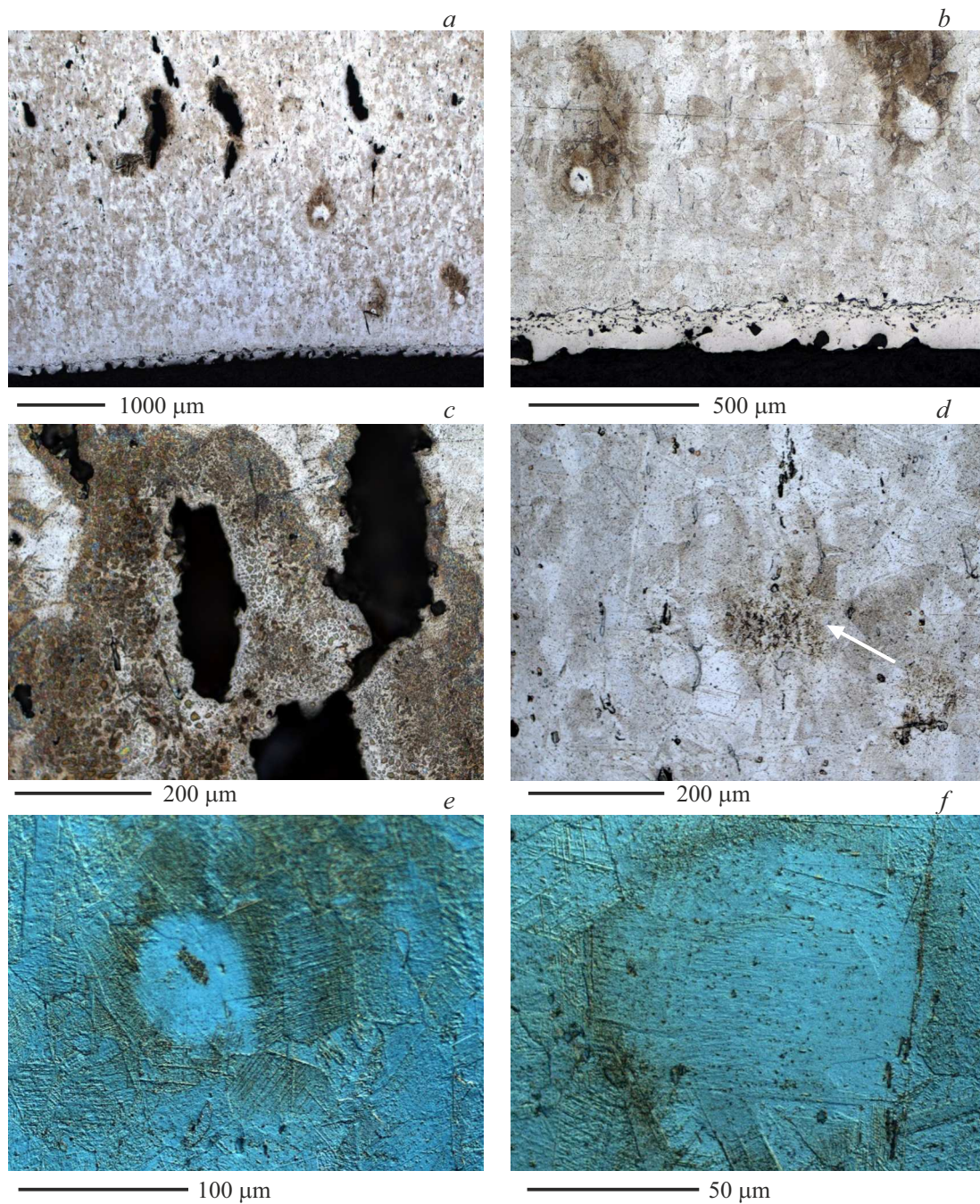


**Figure 13.** Structure of steel 18Cr10NiTi after laser exposure and impact loading at speed of 301 m/s: *a*)  $\times 25$ , *b*)  $\times 100$ , *c* and *d*)  $\times 200$ , *e*)  $\times 500$  C.DIC, *f*)  $\times 1000$  C.DIC).

**Table 2.** Quantitative characteristics of steel 18Cr10NiTi structure after laser processing and impact loading

| Steel            | $V$ , m/s     | Layer, $\mu\text{m}$ | $H_{\text{tw}} \times L_{\text{tw}}$ , $\mu\text{m}$ | $S_{\text{TA}}$ , $\text{m}^{-1}$ |
|------------------|---------------|----------------------|--|-----------------------------------|
| Steel Cr18Ni10Ti | 343 (initial) | 0                    | $1.0 \times 13.7$                                    | $0.76 \cdot 10^6$                 |
|                  | 276           | 79.4                 | $2.9 \times 36.5$                                    | $0.47 \cdot 10^6$                 |
|                  | 304 (polish)  | —                    | $1.5 \times 14.2$                                    | $0.58 \cdot 10^6$                 |
|                  | 301           | 125.7                | $5.7 \times 31.4$                                    | $0.55 \cdot 10^6$                 |

Note. Layer — laser layer thickness,  $V$  — loading rate,  $H_{\text{tw}} \times L_{\text{tw}}$  — twins size,  $S_{\text{TA}}$  — specific surface of twin-austenite phases interface.

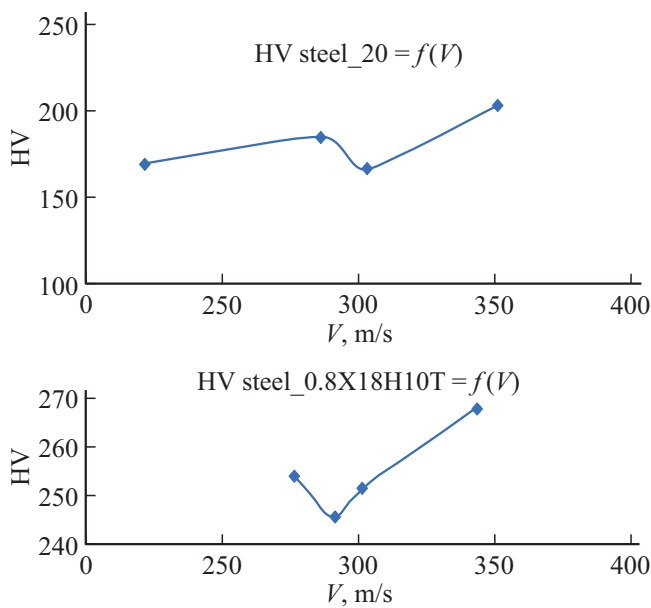


**Figure 14.** Change in hardness of steel 20 and steel 08Cr18Ni10T depending on loading rate.

number of cracks and dendritic structure, as well as areas of amorphization, which have very different hardness, although the average hardness of this sample was found to be quite high.

Figure 14 shows a comparison of the change in hardness of steel 20 and steel 08Cr18Ni10T depending on the loading rate.

The general trend is increase in hardness with loading rate increasing. The decrease in hardness in steel 20 at loading rate of 303 m/s compared to the sample loaded at rate of 286 m/s can be explained by the presence of cracks in the laser layer, despite the maximum amount of martensite in this sample. The drop in hardness in stainless steel at rate of 291 m/s after the laser layer grinding is probably due to the presence of cracks from the surface of the ground laser layer.

## 4. Conclusion

The following main results were obtained in this study.

1. Cold gas-dynamic spraying of the back surface of the target followed by laser processing of steel samples, both carbon and austenitic, leads to slight increase in its dynamic (spallation) strength; this is due to the martensite presence in carbon steel and large number of twins in austenitic steel.

2. Coating has little effect on the dynamic strength of steel 20. The presence of a laser processed layer leads to increase in the amount of martensite in carbon steel, and in austenitic steel to increase in the size of twins and decrease in their number, which leads to increase in hardness regardless of the impact speed.

3. With increase in the loading rate, an increase in the hardness of both carbon steel 20 and austenitic

steel 18Cr10NiTi is observed, while the hardness of the laser layer significantly exceeds the hardness of the base metal.

4. Areas of amorphization in austenitic steel are located near the laser layer, which is associated with the effect of laser processing, and dendritic structure and melting are observed near spallation cracks.

## Conflict of interest

The authors declare that they have no conflict of interest.

## References

- [1] S.V. Klinkov, V.F. Kosarev. *Fizicheskaya mezomekhanika*, **22** (5), 3 (27). (in Russian).
- [2] S.V. Klinkov, V.F. Kosarev, A.S. Zhelnina. *Vestn. PNIPU. Aerokosmicheskaya tekhnika* **47**, 135 (2016). (in Russian).
- [3] A.P. Alkhimov, S.V. Klinkov, V.F. Kosarev, V.M. Fomin. *Kholodnoe gazodinamicheskoe napylenie*. Fizmatlit, M., (2010). 536 p. (in Russian).
- [4] P.W. Leech, A.W. Batchelor, G.W. Stachowiak. *J. Mater. Sci. Lett.* **11**, 16, 1121 (1992).
- [5] *Lazernye tekhnologii obrabotki materialov: sovremennye problemy fundamentalnykh issledovaniy i prikladnykh razrabotok / Pod red. V.Ya. Panchenko*. Fizmatlit, M., (2009). 664 s. (in Russian).
- [6] A.P. Gulyaev. *Metallovedenie. Metallurgiya*, M., (1986). 544 s. (in Russian).
- [7] A.A. Mozhaiko, D.A. Gerashchenkov, M.V. Staritsyn. *Voprosy materialovedeniya*, **2** (110), 44 (2022). (in Russian).
- [8] H. Assadi, H. Kreye, F. Gärtner, T. Klassen. *Acta Mater.* **116**, 382 (2016).
- [9] R.N. Raouf, E. Aubignat, M.-P. Planche, S. Costil, C. Langlade, H. Liao. *Surf. Coat. Technol.* **302**, 47 (2016).
- [10] G. Huang, H. Wang, X. Li, L. Xing, J. Zhou. *Mater. Manuf. Proc.* **33**, 10, 1100 (2018).
- [11] D.A. Gerashchenkov, R.Yu. Bistrov, P.A. Kuznetsov, E.Yu. Gerashchenkova, A.M. Makarov, Yu.M. Markova, A.V. Anisimov. *Voprosy materialovedeniya* **4** (108), 138 (2021). (in Russian).
- [12] K. Baumung, G. Muéller, J. Singer, G.I. Kanel, S.V. Razorenov. *J. Appl. Phys.* **89**, 11, 6523 (2001).
- [13] G.G. Savenkov, A.V. Kuznetsov, A.M. Bragov. *Tech. Phys.* **63**, 5, 718 (2018).
- [14] G.G. Savenkov, A.V. Kuznetsov. *Dynamic characteristics of metallic materials after laser alloying of the surface of samples*. Ch. 8. Monographs „Perspective materials and technologies“. T. 2. Vitebsk: EE „VGTU“, P. 120 (2019).
- [15] V.M. Fomin, A.A. Golyshev, A.G. Malikov, A.A. Filippov, V.S. Shikalov, M.A. Yadrenkin, A.M. Orishich. *J. Eng. Phys. Thermophys.* **7**, 12, 1773 (2022).
- [16] D.A. Gerashchenkov, B.V. Farmakovskiy, A.F. Vasiliev, A.Ch. Mashek. *Voprosy materialovedeniya* **1** (77), 87 (2014). (in Russian).
- [17] V. Gupta, A.S. Argon, D.M. Parks, J.A. Cornie. *J. Mech. Phys. Solids* **40**, 1, 141 (1992).
- [18] L. Davison, D.E. Grady, M. Shahinpoor. *High Pressure Shock Compression of Solids II. Dynamic Fracture and Fragmentation*. Springer, N.Y. (1996).

- [19] L.C. Lev, A.S. Argon. *J. Appl. Phys.* **80**, 1, 529 (1996).
- [20] VI.Vas. Balandin, VI.VI. Balandin, A.M. Bragov, L.A. Igumnov, A.Yu. Konstantinov, A.K. Lomunov. *Mech. Solids* **49**, 6, 666 (2014).
- [21] D.H. Dolan. Foundations of VISAR analysis. SANDIA Report 006–1950. (Printed April 2006).
- [22] Destruction of objects of different scales during an explosion / Ed. A.G. Ivanov. RFNC-VNIIEF, Sarov (2001). 482 p.
- [23] S.A. Saltykov. *Stereometricheskaya metallografiya*. Metallurgiya, M., (1970). 376 s. (in Russian).
- [24] S.N. Buravova, E.V. Petrov. *Russ. J. Phys. Chem. B* **14**, 5, 814 (2020).
- [25] A.F. Belikova, S.N. Buravova, E.V. Petrov. *Vestn. Tambovskogo un-ta. Ser. Estestvennye i tekhnicheskie nauki. Fizika* **21**, 3, 750 (2016). (in Russian).
- [26] S.N. Buravova. *Tech. Phys.* **62**, 10, 1509 (2017).
- [27] A.F. Belikova, S.N. Buravova, E.V. Petrov. *Tech. Phys.* **58**, 8, 1152 (2013).
- [28] A.F. Belikova, S.N. Buravova, Yu.A. Gordopolov. *Tech. Phys.* **58**, 2, 302 (2013).
- [29] S.A. Atroshenko, D.M. Olenin. *Phys. Met. Metallography* **87**, 2, 169 (1999).
- [30] S.A. Atroshenko. *Fizika metallov i metallovedenie 1*, 189 (1991). (in Russian).
- [31] S.N. Buravova, Yu.A. Gordopolov. *Dokl. AN* **417**, 6, 1 (2007). (in Russian).
- [32] S.N. Buravova, Yu.A. Gordopolov, E.V. Petrov, A.V. Poletaev, D.V. Rikhter. *Russ. Metallurgy (Metally)* **2010**, 862 (2010).
- [33] S. Buravova. *Etudes on Theme of the Localization of Dynamic Deformation*. Palmarium Academic Publishing, Saarbrücken (2014). 140 p.
- [34] G.N. Epstein, OA Kaibyshev. *Vysikoskorostnaya deformatsiya i struktura metallov*. (Metallurgiya, M. (1971). 200 s. (in Russian).
- [35] V.I. Zel'dovich, A.E. Kheifets, N.Yu. Frolova, A.K. Muzyrya, A.Yu. Simonov. *Phys. Met. Metallography* **114**, 12, 1031 (2013).
- [36] *Shock Waves and Phenomena of High-Speed Deformation of Metals* / Eds M.A. Meyers, L.E. Murr. Plenum Press, NY (1981). 487 p.
- [37] M.A. Meyers. *Dynamic Behavior of Materials*. John Wiley & Sons, N. Y. (1994). 448 p.

*Translated by I.Mazurov*